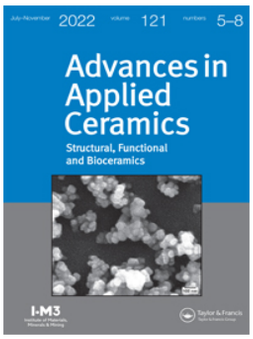

Advances in Applied Ceramics

Structural, Functional and Bioceramics

ISSN: (Print) (Online) Journal homepage: https://www.tandfonline.com/loi/yaac20

The effect of Ti to the crystal structure of $Li_{7-3x}M_xLa_3Zr_{1.8}Ti_{0.2}O_{12}$ (M= Ga, In) garnet-type solid electrolytes as a second dopant

Sevda Saran, Yasin Ramazan Eker, Şule Ateş, Gültekin Çelik, Hadi Baveghar, Osman Murat Özkendir, Ülfet Atav & Wantana Klysubun

To cite this article: Sevda Saran, Yasin Ramazan Eker, Şule Ateş, Gültekin Çelik, Hadi Baveghar, Osman Murat Özkendir, Ülfet Atav & Wantana Klysubun (2022) The effect of Ti to the crystal structure of $Li_{7-3x}M_xLa_3Zr_{1.8}Ti_{0.2}O_{12}$ (M= Ga, In) garnet-type solid electrolytes as a second dopant, Advances in Applied Ceramics, 121:5-8, 238-246, DOI: 10.1080/17436753.2023.2167680

To link to this article: https://doi.org/10.1080/17436753.2023.2167680

View supplementary material

Published online: 23 Jan 2023.

Submit your article to this journal

Article views: 170

View related articles

View Crossmark data

Full Terms & Conditions of access and use can be found at
https://www.tandfonline.com/action/journalInformation?journalCode=yaac20

ADVANCES IN APPLIED CERAMICS
2022, VOL. 121, NOS. 5–8, 238–246
https://doi.org/10.1080/17436753.2023.2167680

I·M3 Institute of Materials, Minerals & Mining
Taylor & Francis
Taylor & Francis Group

RESEARCH ARTICLE

Check for updates

The effect of Ti to the crystal structure of $Li_{7-3x}M_xLa_3Zr_{1.8}Ti_{0.2}O_{12}$ (M= Ga, In) garnet-type solid electrolytes as a second dopant

Sevda Saran[a], Yasin Ramazan Eker[b], Şule Ateş[a], Gültekin Çelik[a], Hadi Baveghar[c], Osman Murat Özkendir[d], Ülfet Atav[a] and Wantana Klysubun[e]

[a]Department of Physics, Faculty of Science, Selçuk University, Konya, Turkey; [b]Faculty of Engineering and Architecture, Department of Metallurgical and Materials Engineering, Necmettin Erbakan University, Konya, Turkey; [c]Nanotechnology and Advanced Materials, Selçuk University, Institute of Science, Konya, Turkey; [d]Faculty of Engineering, Department of Natural and Mathematical Sciences, Tarsus University, Mersin, Turkey; [e]Synchrotron Light Research Institute (SLRI), Nakhon Ratchasima, Thailand

ABSTRACT

Garnet-type solid-state electrolytes are promising candidates for solid-state lithium batteries, nevertheless their ionic conductivity is still not enough for commercial applications. On the other hand, doping still is the common way to improve the ionic conductivities of these solid electrolytes. In this study, mono and dual-doped garnet-type solid electrolytes were synthesised by substituting indium (In), gallium (Ga), indium-titanium (In-Ti) and gallium-titanium (Ga-Ti) to the $Li_7La_3Zr_2O_{12}$ structure by a solid-state reaction method. The contribution of substitutions to the formation of crystal phases was investigated by X-ray diffraction (XRD) and X-ray absorption spectroscopy (XAS). On the other hand, morphological analyses were done by scanning electron microscope (SEM) and the ionic conductivities of the solid electrolytes were determined by electrochemical impedance spectroscopy (EIS). The study showed that while $Li_{7-3x}In_xLa_3Zr_2O_{12}$ (for x = 0.05, 0.10, 0.15, 0.20) and $Li_{7-3x}Ga_xLa_3Zr_2O_{12}$ (for x = 0.05) samples were formed in tetragonal phase with a space group of I41/acd:2, dual substituted $Li_{7-3x}In_xLa_3Zr_{1.8}Ti_{0.2}O_{12}$ and $Li_{7-3x}Ga_xLa_3Zr_{1.8}Ti_{0.2}O_{12}$ solid electrolytes for all x values were formed in cubic phase with a space group of I-43d. The highest conductivity is reached for $Li_{6.85}Ga_{0.05}La_3Zr_{1.8}Ti_{0.2}O_{12}$. The radial distribution function studies showed that when more In and Ga atoms take place in the sites of Li atoms, more O atoms take place in the vicinity of both substituted In and Ga atoms within the $Li_7La_3Zr_{1.8}Ti_{0.2}O_{12}$ (LLZTO) crystal framework which can eventuate in a change in the conduction mechanism.

ARTICLE HISTORY
Received 30 June 2021
Revised 28 September 2022
Accepted 9 January 2023

KEYWORDS
Garnet-type solid electrolytes; solid-state batteries; solid electrolytes; energy

Introduction

Garnet-type $Li_7La_3Zr_2O_{12}$ (LLZO) solid electrolytes have been a focus point since cubic phase is discovered in 2007 [1]. Although these types of solid electrolytes have reached a good conductivity by substituting different cations to the LLZO structure, the challenge is that the ionic conduction is not enough to replace them with liquid-based electrolytes [2–4]. Cubic LLZO which is not stable at room temperature has a conduction of two orders of magnitude higher than that of the tetragonal LLZO [5]. In order to stabilise cubic phase, and get a higher conductivity, different super valent cations are substituted to the LLZO structure. Recent studies have been investigated various substitution of cations such as Al, Ga for Li sites, Nb, Ta for Zr sites and Sr, Y for La sites [6–13]. Although substitution is effective to regulate the crystal structure, different cations doped to different sites of LLZO have distinct influences on the electronic structure, the local atomic environment, the size of lithium-ion channels, the density, etc. It has been reported that partial replacement of Zr^{4+} sites by a smaller-sized Ti^{4+} is highly effective to modulate the Li^+ distribution and to increase the density of the LLZO structure, which is favourable to improve the ionic conductivity [14]. Additionally, it has been proved that doping of Li^+ by Al^{3+}, Ge^{4+} and Ga^{3+} can also boost the Li^+ conductivity by getting a higher Coulombic repulsion between doped cations and Li^+ ions [15–17]. On the other hand, partially replacing of La^{3+} ions with larger ion diameter dopants such as Sr^{2+} increases the Li^+ ion transport channels by enlarging the bottleneck size of Li^+ ion migration channels, eventually enhancing the mobility of Li^+ ions and the conduction [18]. All these studies reveal that each doping strategy within different ionic sites in LLZO structure has an effective role in the reformation of the structure. Therefore, until now researchers developed new strategies like multistep cation doping process, or simultaneously doping to achieve the highest possible Li^+ conductivity with an optimised structure [19–23].

CONTACT Sevda Saran sevdaaktas@selcuk.edu.tr
Supplemental data for this article can be accessed online at https://doi.org/10.1080/17436753.2023.2167680.
© 2023 Institute of Materials, Minerals and Mining. Published by Taylor & Francis on behalf of the Institute.

In this work, mono $Li_{7-3x}M_xLa_3Zr_2O_{12}$ (M = Ga, In) (x = 0.05, 0.10, 0.15, 0.20) and dual doped $Li_{7-3x}M_xLa_{3-}Zr_{1.8}Ti_{0.2}O_{12}$ (LLZTO) (M = Ga, In) (x = 0.00, 0.05, 0.10, 0.15, 0.20) garnet-like structures were synthesised by a solid-state reaction method. Samples formed in a cubic phase when 20% of Ti^{4+} was incorporated into the Zr^{4+} sites simultaneously as a second dopant. The effects of dopants on the crystal structure, ionic conductivity, morphology, local environment and electronic structure were investigated via respectively powder X-ray diffraction (XRD), electrochemical impedance spectroscopy (EIS), scanning electron microscopy (SEM), and X-ray absorption spectroscopy (XAS).

Experimental

$Li_{7-3x}In_xLa_3Zr_2O_{12}$, $Li_{7-3x}Ga_xLa_3Zr_2O_{12}$, (x = 0.05, 0.10, 0.15, 0.20) and $Li_{7-3x}Ga_xLa_3Zr_{1.8}Ti_{0.2}O_{12}$, $Li_{7-3x-}In_xLa_3Zr_{1.8}Ti_{0.2}O_{12}$ (x = 0.00, 0.05, 0.10, 0.15, 0.20) samples were synthesised by a series of ball milling and heat treatment processes as described in reference [24].

Crystalline structure of the samples was studied by XRD patterns which taken by Bruker D8 X-ray diffractometer with CuKα source. Morphology of the samples was examined by SEM using a ZEISS LS 10 model microscope. For the EIS measurements, the powders were pressed as pellets those have a thickness of 0.9–1 mm and a diameter of 12 mm. In order to have ionically blocking electrodes both sides of pellets were coated with Ag paste. EIS measurements were taken by Gamry PCI4/750 Potentiostat in the frequency range of 10^{-1}–10^5 Hz at room temperature. The electronic structure analysis and its impact on the crystal structure of the studied materials are carried out by the collected X-ray absorption fine structure (XAFS) data from the BL8:XAS beamline of the SIAM Photon synchrotron laboratory (SLRI) which is located in Suranaree University, Nakhon Ratschasima, Thailand [25]. The data analysis was carried on two parts: XANES (X-ray Absorption Near Edge Spectroscopy) for the electronic properties and EXAFS (Extended-XAFS) for structural characterization in the materials. The EXAFS data were extracted from the tail part of the collected XAFS spectra and processed with the software of IFEFFIT package [26].

Results and discussion

Structural analysis

A series of different element doping procedure were performed to probe the crystal structure formation of LLZO. Figure 1 represents the XRD patterns for the samples with different mono and dual-doped elements and quantities. The crystal structure of $Li_{7-3x}In_xLa_3Zr_2O_{12}$ (Figure 1(a)) is stable at typical tetragonal phase independently of In substitution amount, however for the sample $Li_{7-3x}Ga_xLa_3Zr_2O_{12}$ (Figure 1(b)), when the amount of Ga substitution reaches a critical value of 10%, the structure captures the cubic phase. Moreover, In-doped tetragonal LLZO shows a secondary phase $La_2Zr_2O_7$ at $2\theta = 28.88^o$ which is a common impurity phase in the literature [27,28]. On the other hand, the incorporation of Ti in the Zr sites by 20% brings out amendments in the crystal structures. Under the same experimental conditions, when a portion of Zr is displaced by substituting Ti, the 5% Ga and all the In-doped tetragonal LLZO structures undergo a phase transition to a cubic phase. Furthermore, no additional peaks i.e. any other compound or impurity are observed within the diffractograms (Figure 1(c,d)).

To designate the crystal structure of LLZO, Rietveld analyses were applied to the XRD data by using the MAUD software, and the results are illustrated in Table 1. Crystal structure analysis yielded lattice parameters as a = 12.93–12.97 Å with a space group of I-43d for Ga-doped cubic $Li_{7-3x}Ga_xLa_3Zr_2O_{12}$ (x = 0.10, 0.15, 0.20), a = 13.02–13.04 Å, c = 12.66–12.70 Å with a space group of I41/acd:2 for In-doped tetragonal $Li_{7-3x}In_xLa_3Zr_2O_{12}$ (x = 0.05, 0.10, 0.15, 0.20), a = 12.89–12.92 Å with a space group of I-43d for dual In-Ti doped cubic $Li_{7-3x}In_xLa_3Zr_{1.8}Ti_{0.2}O_{12}$ (x = 0.00, 0.05, 0.10, 0.15, 0.20) and a = 12.92–12.94 Å with a space group of I-43d for dual Ga-Ti doped cubic $Li_{7-3x}Ga_xLa_3Zr_{1.8}Ti_{0.2}O_{12}$ (x = 0.00, 0.05, 0.10, 0.15, 0.20).

It is believed that the stabilization of the cubic phase is obtained by increasing the Li vacancies in the LLZO [29]. Here dual doping strategy is used as an alternative way to stabilize the cubic structure. Both structures doped either with 5% Ga or 5–20% In are tetragonal. However, when the dual substitution takes place by the introduction of Ti, only the cubic LLZO phase appears. These results confirm the role of Ti for the stabilization of the cubic phase. Ti probably decreases the free energy of the crystal down to the formation of the cubic structure [19]. Sample's crystal lattice parameters at different substituent concentrations showed unusual Vegard's behaviour without a linear change of the lattice parameter. The possible reason for this phenomenon is due to the oxygen coordination shell surrounding the local and doped metals varying the amount of dopants. The high electronegativity of the oxygen atoms has strong effects on the outer shell electrons of the atoms located in its close vicinity, causing the formation of tightly bound oxide structures with high coupling.

Morphological analysis

Morphology of the doped LLZO powders was examined by SEM. Micrographs of the samples Li_{7-}

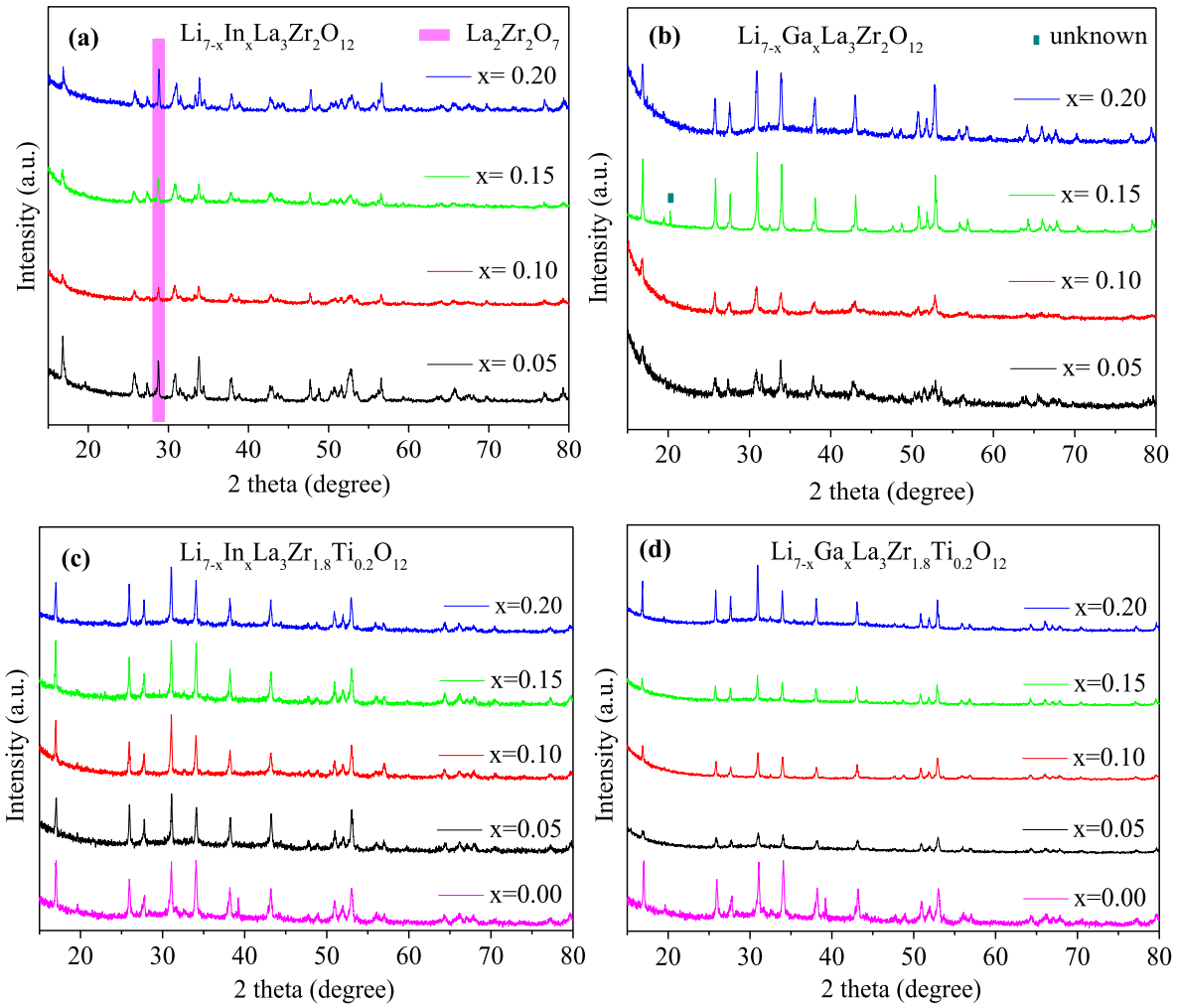

Figure 1. XRD patterns for solid electrolytes (a) $Li_{7-3x}In_xLa_3Zr_2O_{12}$, (b) $Li_{7-3x}Ga_xLa_3Zr_2O_{12}$ (x = 0.05, 0.10, 0.15, 0.20), (c) $Li_{7-3x}In_xLa_3Zr_{1.8}Ti_{0.2}O_{12}$, (d) $Li_{7-3x}Ga_xLa_3Zr_{1.8}Ti_{0.2}O_{12}$ (x = 0.00, 0.05, 0.10, 0.15, 0.20).

$_{3x}In_xLa_3Zr_2O_{12}$ and $Li_{7-3x}Ga_xLa_3Zr_2O_{12}$ (for x = 0.05, 0.10), $Li_{7-3x}In_xLa_3Zr_{1.8}Ti_{0.2}O_{12}$ and $Li_{7-3x}Ga_xLa_3Zr_{1.8}Ti_{0.2}O_{12}$ (for x = 0.00, 0.05, 0.10) are shown in Figure 2. For the tetragonal and cubic particles, a distinct change in the morphology of the microstructure was observed. The microstructure of the tetragonal $Li_{7-3x}In_xLa_3Zr_2O_{12}$ (Figure 2(a, b)) samples appears to be a combination of irregular-sized particles with large and small ones that approves formation of the second phase ($La_2Zr_2O_7$), while the tetragonal Ga-doped LLZO particles (Figure 2(c, d)) show a smooth surface. On the other hand, the cubic In-Ti (Figure 2(f, g)) and Ga-Ti (Figure 2(i, j)) doped LLZO particles show a relatively similar microstructure with cubic Ti-doped (Figure 2(e, h)) LLZO particles. Furthermore, no more small particles are observed with In-Ti (Figure 2(f, g)) doped LLZO structure, suggesting the sample is in a pure phase.

Impedance measurements

Room temperature impedance data were taken to study the ionic conductivity of the samples and are illustrated in Figure 3. In this figure, we present mono and dual doped LLZO samples for x = 0.05 to investigate the effect of Ti. To fit the experimental data two different equivalent circuits are used. The first one shown in Figure 3(e) is used for In, Ga and In-Ti doped samples (Figure 3(a–c)), and the second one shown in Figure 3(f) is used for Ga-Ti doped sample (Figure 3(d)). The last part of the equivalent circuits consists of a charge transfer resistance ($R_{ct.}$), a Warburg element (W) and a constant phase element attributed to the double layer ($CPE_{dl.}$) between pellet and silver electrodes. Since this part is related to the physical region formed between the interface of LLZO and the silver electrodes, it is not considered for the conductivity calculations of the mono and dual-doped LLZO samples. The abbreviations of R_{bulk}, $R_{gb.}$, CPE_{bulk} and $CPE_{gb.}$ in the first part of the equivalent circuits state bulk and grain boundary resistivity, bulk and grain boundary constant phase elements, respectively. Constant phase element which is an imperfect capacitance has a complex impedance defined as, $Z_{CPE} = 1/Q(jw)^n$, where Q (or CPE) has a unit of Ss^n (siemens seconds to the power n),

Table 1. Rietveld analysis results of the $Li_{7-3x}M_xLa_3Zr_2O_{12}$, $Li_{7-3x}M_xLa_3Zr_{1.8}Ti_{0.2}O_{12}$ (M = In, Ga) samples.

Substitution	Crystal	a (Å)	c (Å)	Geometry	SG	% (Weight)
$Li_{7-3x}In_xLa_3Zr_2O_{12}$						
x = 0.05	$Li_{6.85}In_{0.05}La_3Zr_2O_{12}$	13.04	12.67	Tetragonal	I41/acd:2	94.66
	$La_2Zr_2O_7$	10.81	–	Cubic	Fd-3m:2	5.34
x = 0.10	$Li_{6.70}In_{0.10}La_3Zr_2O_{12}$	13.04	12.70	Tetragonal	I41/acd:2	92.33
	$La_2Zr_2O_7$	10.78	–	Cubic	Fd-3m:2	7.67
x = 0.15	$Li_{6.55}In_{0.15}La_3Zr_2O_{12}$	13.04	12.70	Tetragonal	I41/acd:2	93.30
	$La_2Zr_2O_7$	10.80	–	Cubic	Fd-3m:2	6.70
x = 0.20	$Li_{6.40}In_{0.20}La_3Zr_2O_{12}$	13.02	12.66	Tetragonal	I41/acd:2	94.37
	$La_2Zr_2O_7$	10.81	–	Cubic	Fd-3m:2	5.63
$Li_{7-3x}Ga_xLa_3Zr_2O_{12}$						
x = 0.05	$Li_{6.85}Ga_{0.05}La_3Zr_2O_{12}$	13.04	12.65	Tetragonal	I41/acd:2	100
x = 0.10	$Li_{6.70}Ga_{0.10}La_3Zr_2O_{12}$	12.96	–	Cubic	I-43d	100
x = 0.15	$Li_{6.55}Ga_{0.15}La_3Zr_2O_{12}$	12.93	–	Cubic	I-43d	100
x = 0.20	$Li_{6.40}Ga_{0.20}La_3Zr_2O_{12}$	12.97	–	Cubic	I-43d	100
$Li_{7-3x}In_xLa_3Zr_{1.8}Ti_{0.2}O_{12}$			–			
x = 0.00	$Li_7La_3Zr_{1.8}Ti_{0.2}O_{12}$	12.90	–	Cubic	Ia-3d	100
x = 0.05	$Li_{6.85}In_{0.05}La_3Zr_{1.8}Ti_{0.2}O_{12}$	12.89	–	Cubic	I-43d	100
x = 0.10	$Li_{6.70}In_{0.10}La_3Zr_{1.8}Ti_{0.2}O_{12}$	12.89	–	Cubic	I-43d	100
x = 0.15	$Li_{6.55}In_{0.15}La_3Zr_{1.8}Ti_{0.2}O_{12}$	12.92	–	Cubic	I-43d	100
x = 0.20	$Li_{6.40}In_{0.20}La_3Zr_{1.8}Ti_{0.2}O_{12}$	12.91	–	Cubic	I-43d	100
$Li_{7-3x}Ga_xLa_3Zr_{1.8}Ti_{0.2}O_{12}$			–			
x = 0.00	$Li_7La_3Zr_{1.8}Ti_{0.2}O_{12}$	12.90	–	Cubic	Ia-3d	100
x = 0.05	$Li_{6.85}Ga_{0.05}La_3Zr_{1.8}Ti_{0.2}O_{12}$	12.92	–	Cubic	I-43d	100
x = 0.10	$Li_{6.70}Ga_{0.10}La_3Zr_{1.8}Ti_{0.2}O_{12}$	12.93	–	Cubic	I-43d	100
x = 0.15	$Li_{6.55}Ga_{0.15}La_3Zr_{1.8}Ti_{0.2}O_{12}$	12.94	–	Cubic	I-43d	100
x = 0.20	$Li_{6.40}Ga_{0.20}La_3Zr_{1.8}Ti_{0.2}O_{12}$	12.93	–	Cubic	I-43d	100

$j = \sqrt{-1}$ and n is a constant. Total ionic conductivities of the pellets were estimated from the equation: $\sigma_t = (1/R_t)(l/A)$, where σ_t, R_t, l and A indicate total ionic conductivity, total resistivity ($R_{bulk} + R_{gb.}$), thickness and the area of the pellet, respectively.

The values of R_{bulk}, $R_{gb.}$, Q_{bulk}, $Q_{gb.}$, n_{bulk} and $n_{gb.}$ calculated from the fitted results (Gamry Echem Analyst software) are presented in Table 2.

From a general point of view, when the total resistivities in Table 2 are compared, the LLZO conductivity is better with Ga doping than In. The conductivity of $Li_{6.85}Ga_{0.05}La_3Zr_2O_{12}$ is 3.04×10^{-6} S.cm^{-1}, while it is 1.23×10^{-7} S.cm^{-1} for $Li_{6.85}In_{0.05}La_3Zr_2O_{12}$. The equivalent circuit element (R_{bulk} and R_{gb}) values of only Ga-doped LLZO are lower by one order compared to those of only In-doped LLZO. These results show that the presence of In reduces the ionic conductivity within the structure. Since the electronegativity of In (1.78) is lower than the one of Ga (1.8), the increase in bulk capacity is not due to an electronic trap that could be created by In, but probably due to the change in the lattice parameter. On the other hand, with the Ti co-doping, the bulk resistivity (R_{bulk}) of the Ga-doped LLZO is divided by four and no bulk capacitive value has been detected. However, despite the almost constant grain boundaries resistivity ($R_{gb.}$), the capacitive constant of the grain boundaries increases involving an increase of the impedance of grain boundaries. This increase of grain boundaries impedance is counteracted by the improvement due to the reduction of the bulk impedance involving a slightly better conductivity of Ga-Ti doped LLZO, 3.06×10^{-6} S.cm^{-1}. Finally, the introduction of Ti within the In doped LLZO involves an increase of the bulk and grain boundaries impedance that negatively affect the conductivity of In-Ti doped LLZO with decrease down to 2.58×10^{-8} S.cm^{-1}.

Electronic structural properties

The LLZO material is a popular solid state electrolyte material containing four different elements, which have strong bonding with each other. The doping with Ga^{3+} forced to replace three Li^+ within the LLZO structure. On the other side, the co-doping of Ga and Ti greatly improve the conductivity within the grains. In order to better understand the effect of these substitution especially on the electronic structure, $Li_{7-3x}Ga_xLa_3Zr_{1.8}Ti_{0.2}O_{12}$ (x = 0.10, 0.20) samples have been characterised by XANES spectroscopy. The gallium K-edge XANES spectra of the substituted Ga^{3+} in LLZTO materials are given in Figure 4. α-Ga_2O_3 material is used as a reference for comparison of the absorption data. The high compatibility of the absorption edge data of the Ga-doped materials with the main spectrum peak and the outline of the reference material gallium K-edge show that the Ga atoms doped into LLZTO have similar conditions to the oxidation and chemical environment in the α-Ga_2O_3 material. However, the post-edge asymmetries highlight a different geometry than the LLZTO structures.

The K-edge absorption spectra of the gallium atom is a result of the excitation of the 1s electrons to the empty levels above the valence levels. As the electronic configuration of the Ga^{3+} ions are [Ar] $4s^0$ $3d^{10}$, the 4p levels are totally unoccupied. So, the route for the excited electrons are 1s→4p. The main absorption

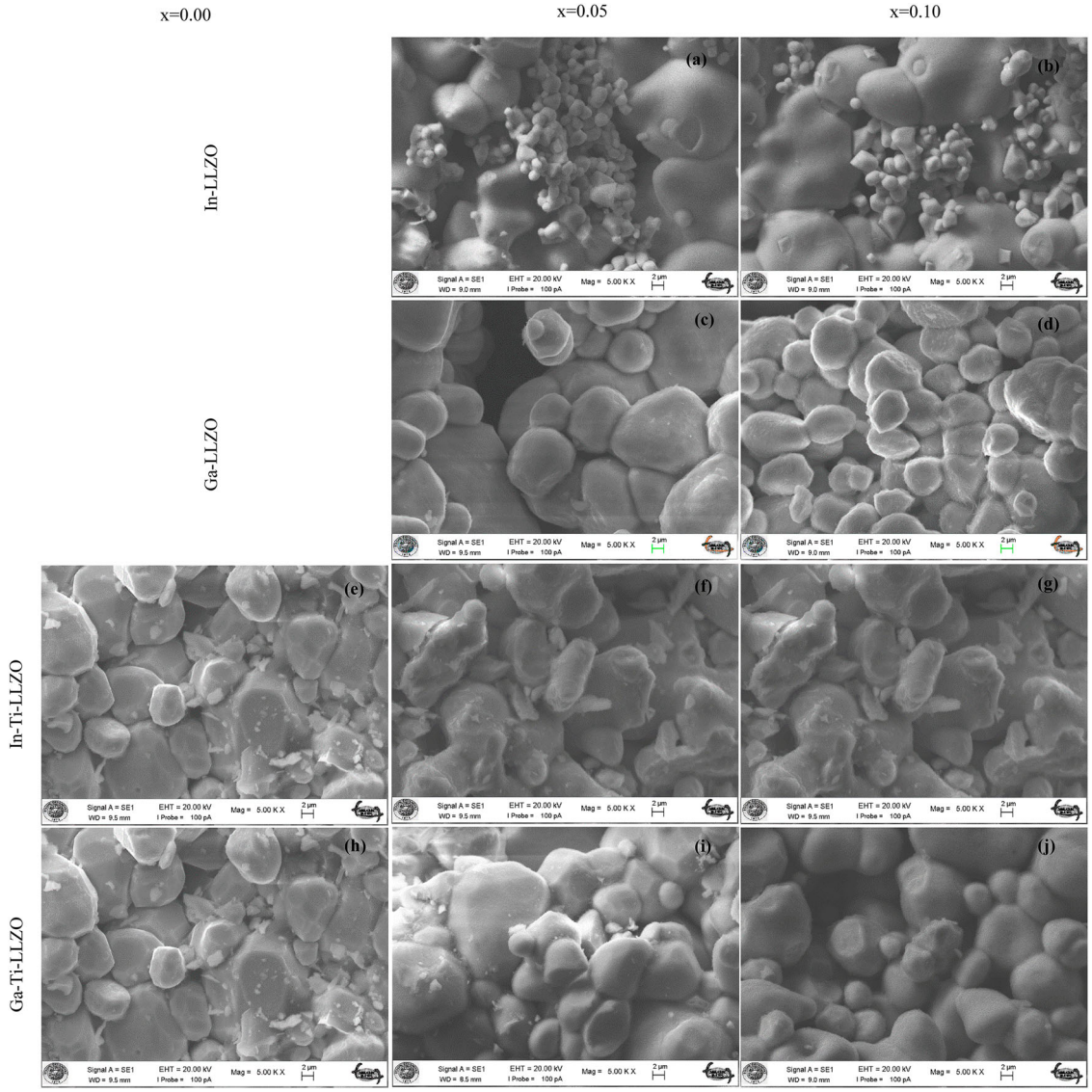

Figure 2. SEM micrographs of the solid electrolytes (a–b) $Li_{7-3x}In_xLa_3Zr_2O_{12}$, (c–d) $Li_{7-3x}Ga_xLa_3Zr_2O_{12}$ (e–f–g) $Li_{7-3x}In_xLa_3Zr_{1.8}Ti_{0.2}O_{12}$, (h–i–j) $Li_{7-3x}Ga_xLa_3Zr_{1.8}Ti_{0.2}O_{12}$, first columb is for x = 0.00, the second columb is for x = 0.05 and the third columb is for x = 0.10.

edge of the samples has a high compatibility with peak property at 10,371.5 eV. The post-edges at 10,382.9 eV indicate different amount of Ga atoms in the LLZTO structure, where a portion of the substituted Ga atoms tends to form a different site symmetry due to the influence of the electronic interaction that yield d-d metal bonding via their neighbouring atoms.

The peak structures after 10,400 eV are the interference of the wave functions of the excited photoelectrons that occur during the multiple scattering process in the zone of the nearest neighbouring atoms. The extraction of these structures through X-ray absorption spectra yields information about the photoelectron's scattering among neighbouring atoms and can be analysed via the EXAFS scattering equation [30,31].

$$\chi = [\mu(E) - \mu_o(E)/\Delta\mu_o] \quad (1)$$

Here, μ represents the absorption coefficient. EXAFS scattering intensities of photoelectrons emitted from gallium atom, a member of LLZTO material, are extracted from collected XAFS data via the ATHENA software and processed by the ARTEMIS software. The scattering intensities and the k^2 multiplied scattering intensities of the reference and Ga substituted LLZTO materials are given in Figure S1.

Synchronous data fluctuations emphasise the similar ordering of gallium atoms in the crystals. The multiplication of scattering intensities (Figure S1(a)) with k^2 (Figure S1(b)) involves a big jump at high k values. Since the signals come from heavier atoms jump more than the other ones, the multiplication by the power of k reveals big atoms around Ga atoms. In other words, distortion at high k values of scattering intensities emphasizes a strong interatomic potential which causes a high decrease in the kinetic energy of

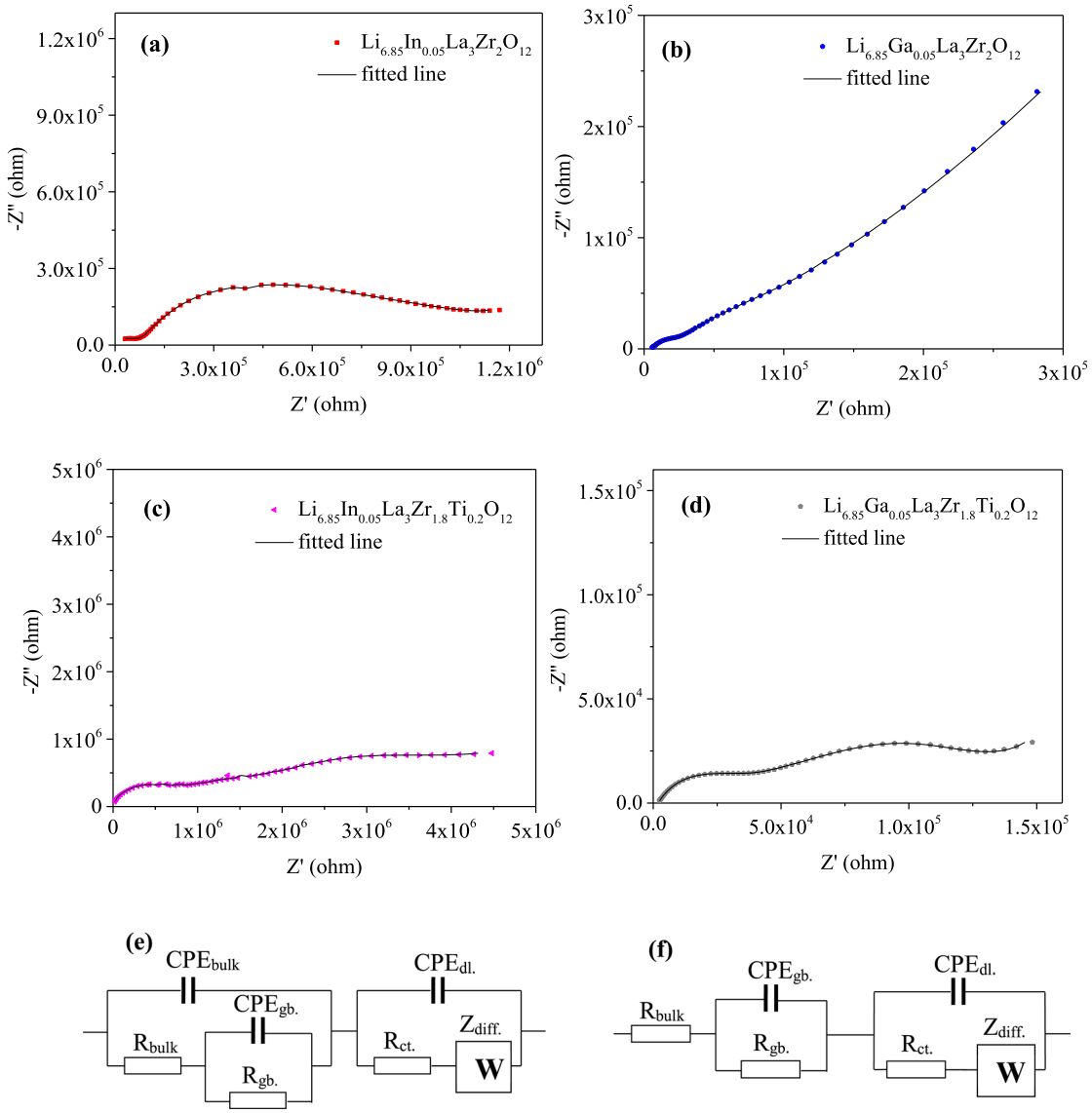

Figure 3. Nyquist plots of the impedance spectra and fitted data for (a) $Li_{6.85}In_{0.05}La_3Zr_2O_{12}$, (b) $Li_{6.85}Ga_{0.05}La_3Zr_2O_{12}$, (c) $Li_{6.85}In_{0.05}La_3Zr_{1.8}Ti_{0.2}O_{12}$, and (d) $Li_{6.85}Ga_{0.05}La_3Zr_{1.8}Ti_{0.2}O_{12}$, (e) The equivalent circuit model used to fit experimental data of the In, In-Ti and Ga-Ti (Figure 3(a, b, c) doped LLZO, (f) The equivalent circuit model used to fit experimental data of the Ga-Ti (Figure 3(d)) doped sample.

photoelectrons travelling between neighbouring atoms. Besides, high agreement between the Ga substituted materials data confirms the preserved crystal structure in both materials. However, a tiny shift on the 20% Ga substituted samples points out a variation in the crystal density due to the increasing Ga substitution.

Fourier transformations of EXAFS (FT-EXAFS) scattering intensity provide the radial distribution of atoms on a one-dimensional axis around the absorbing gallium atoms in the X-ray absorption spectrum. The data yielded from the Fourier transformation process can also be called as the radial distribution function (RDF) in real space and gives us the distances in one-dimensional axis. The distances of atoms from the source atom (Ga) on one-dimensional axis is given in Figure 5. The first data in the figure (black) belongs to the reference material α-Ga_2O_3, while the red and green data refer to the Ga-doped LLZTO materials. The data of the reference α-

Table 2. The values of the equivalent circuit elements obtained by fitting the impedance spectra in Figure 3(a–d). Here, χ^2 is the square of the standard deviation.

Sample	R_{bulk} (Ω)	$R_{gb.}$ (Ω)	$Q_{bulk}(Ss^n)$	$Q_{gb.}$ (Ss^n)	n_{bulk}	$n_{gb.}$	χ^2
$Li_{6.85}In_{0.05}La_3Zr_2O_{12}$	7.87×10^4	6.54×10^5	3.17×10^{-7}	2.05×10^{-8}	5.3×10^{-1}	8.07.x10^{-1}	1.25×10^{-4}
$Li_{6.85}Ga_{0.05}La_3Zr_2O_{12}$	6.02×10^3	2.25×10^4	1.37×10^{-7}	2.32×10^{-10}	7.64×10^{-1}	6.84×10^{-1}	3.22×10^{-5}
$Li_{6.85}In_{0.05}La_3\ Zr_{1.8}Ti_{0.2}O_{12}$	4.39×10^5	4.18×10^6	9.92×10^{-8}	6.04×10^{-11}	3.25×10^{-1}	9.16×10^{-1}	1.05×10^{-3}
$Li_{6.85}Ga_{0.05}La_3\ Zr_{1.8}Ti_{0.2}O_{12}$	1.63×10^3	2.58×10^4	–	2.97×10^{-8}	–	8.16×10^{-1}	1.22×10^{-4}

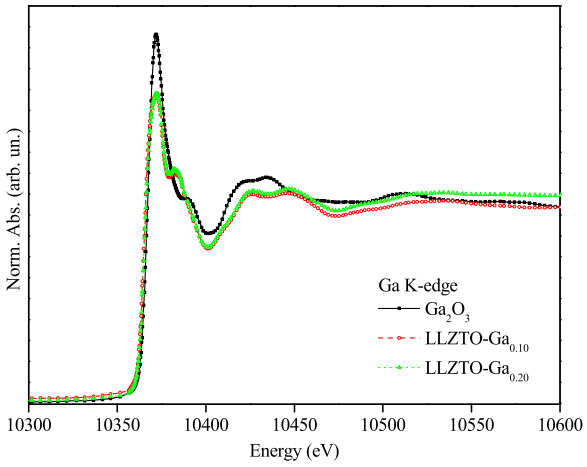

Figure 4. The Ga K-edge XANES comparison of the Ga substituted LLZTO materials.

Ga_2O_3 and 10% doped materials match the average number of peaks, however, it is remarkable that the 20% doped material has more peaks. The main reason for this can be the decomposition resulting from the variation in the oxygen bonding and numbers of oxygen in the bulk due to Ga concentrations.

The presence of gallium atoms in the LLZTO attracted more oxygen in its vicinity, and the different oxidation properties of the Ga atom cause more peaks in the RDF structure of the regional atomic settlements in the crystal structure. This is a result of the higher electronegativity values of the gallium (electronegativity value is app. 1.8), that sits in the three Li (electronegativity value is app. 1.0) ions coordination [32,33]. Unlike the reference α-Ga_2O_3 structure, with increasing the number of Ga atom in the LLZTO crystal, more oxygen atoms find place closer to the Ga atom which sits at the origin, i.e, more oxygen atoms are located between metals. The increasing number of RDF peaks and the weaker peak intensities in other samples can also emphasise the change in the bonding angles of oxygen atoms.

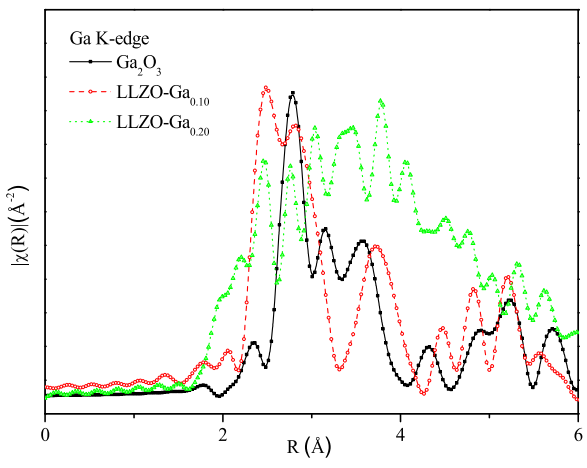

Figure 5. RDF of the Ga K-edge scattering intensities.

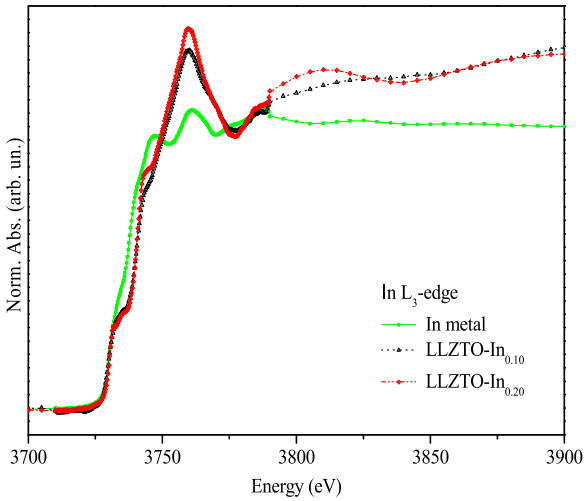

Figure 6. The In L_3-edge XANES comparison of the substituted LLZTO materials.

In Figure 6, the normalized absorption edge spectra of In L_3 of different In-doped materials are given in comparison with the reference data taken from indium metal. Spectra from reference In metal and the indium-doped samples show similarities in their electronic structure. The increase in the normalized intensity of the peaks is related to the unoccupied states of the excited $2p_{3/2}$ electrons that can transit as a final state. The more uniform spectral structure of the metal indicates the uniformly distributed and single crystal structure presented in the material. Regarding the LLZTO samples, L_3 absorption spectrum is due to the transition of the $2p_{3/2}$ core level electrons to the empty 5s level, which is governed by the quantum selection rules. Here, the main absorption edge is divided into two main parts, the peak structures at 3747 and 3761 eV are the result of different crystal symmetries occurring within the material. However, the transition to the empty 5p levels below the 5s level is forbidden by the selection rules. Although the overlap between the p-s levels that were close to each other (in terms of energy) was weak, the transition of the core level electrons is allowed to the lower energy levels of these energies. Therefore, two peak structure (low-energy (t_{2g}) and high-energy (e_g)) were formed in the pre-edge region below the main absorption edge at an energy value of 3731 eV.

The comparison of the EXAFS spectra obtained from the indium-substituted LLZTO materials with the indium metal foil is given in Figure S2. The correlation between the scattering intensity data from 10% In substituted LLZTO material and the scattering spectrum from 20% In substituted LLZTO material is remarkable. Furthermore, degradation of high *k* values emphasises a strong interatomic potential, which causes a high decrease in kinetic energy of photoelectrons travelling between neighbouring

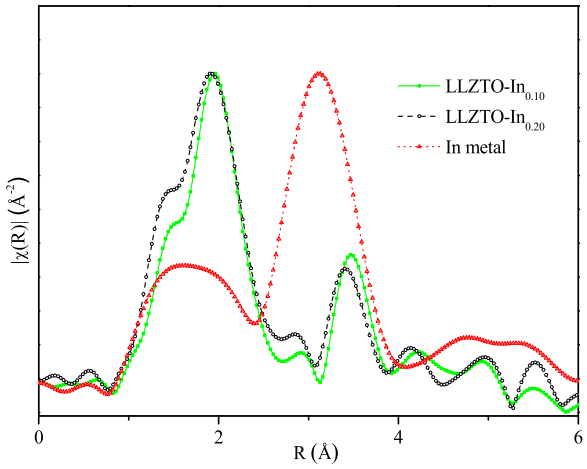

Figure 7. The radial distribution function of the In L_3-edge scattering intensities.

atoms. From the Figure S2 (b) which is the square power of *k* of the scattering intensity, it is estimated that the strong interatomic potential around the substituted In atoms is caused by the big atoms such as La.

Fourier transforms of the scattering intensity of EXAFS provide the radial distribution of the atoms around the indium atoms, where the photoelectrons are emitted [34]. The radial distribution of atoms on a one-dimensional axis is given in Figure 7. The red plot in the figure is the data belonging to the metal indium foil as the reference material, while the black and green data refer to In substituted LLZTO materials. The data of 20% and 10% substituted material show high agreement with matched peak numbers, and a slight peak shifts to the origin is observed due to the push of the heavier indium atoms on its neighbouring atoms with the increase in amount. However, broader peak features are obvious in 20% substituted material which is a result of more overlapped peaks. The reasons for such overlapped data are; atoms may have been placed at the same distances with different azimuthal angles or, they may have different positions but very close distances to each other.

Conclusion

In conclusion, dual substitution method was applied to the garnet-type solid electrolyte to investigate the crystal structure and conduction mechanism changes within this sample. While mono doped $Li_{7-3x}In_xLa_3Zr_{1.8}O_{12}$ sample was formed in the tetragonal phase, dual doped $Li_{7-3x}In_xLa_3Zr_{1.8}Ti_{0.2}O_{12}$ and $Li_{7-3x}Ga_xLa_3Zr_{1.8}Ti_{0.2}O_{12}$ samples tended to form in the cubic phase. Synchronous data fluctuations in the EXAFS scattering intensities also supported that Ga-Ti doped solid electrolytes were formed in the same crystal structures for all amounts of Ga. Besides, the high symmetry on the absorption edge structures in each In-Ti doped solid electrolytes, where a change in the In amounts was treated, also confirmed the stability in their crystal structure, even the change in In amounts.

EIS measurements showed that the Ga and Ga-Ti doped solid electrolytes have almost the same ionic conductivity, however In-Ti doped LLZO has 4.77 times lower ionic conductivity than In-doped LLZO. Although Ti is effective for the transformation of tetragonal phase to the cubic phase, it is not effective to improve the ionic conductivity as a second dopant. With the comparison of previous studies in the literature, the ionic conductivity is not improved, but it is believed that this study will contribute to the improvement of dual doping strategy.

Acknowledgements

The authors gratefully acknowledge the financial support of '17101004' project of Selçuk University Scientific Research Projects (BAP) Coordinating Office (Konya, Turkey).

Disclosure statement

No potential conflict of interest was reported by the author(s).

Funding

This work was supported by Selçuk University Research Foundation [grant number 17101004].

References

[1] Murugan R, Thangadurai V, Weppner W. Fast lithium ion conduction in garnet-type $Li_7La_3Zr_2O_{12}$. Angew Chem, Int Ed. 2007;46(41):7778–7781.
[2] Buannic L, Naviroj M, Miller SM, et al. Dense freeze-cast $Li_7La_3Zr_2O_{12}$ solid electrolytes with oriented open porosity and contiguous ceramic scaffold. J Am Ceram Soc. 2019;102(3):1021–1029.
[3] Kotobuki M, Munakata H, Kanamura K, et al. Compatibility of $Li_7La_3Zr_2O_{12}$ solid electrolyte to all-solid-state battery using Li metal anode. J Electrochem Soc. 2010;157(10):A1076–A1079.
[4] Thangadurai V, Chen B. Solid Li- and Na-Ion electrolytes for next generation rechargeable batteries. Chem Mater. 2022;34(15):6637–6658.
[5] Yan SH, Cui Q, Sun C, et al. Enhancing the ionic conductivity and stabilizing cubic structure of garnet-type $Li_{6.25-x}Al_{0.25}La_3Zr_{2-x}Ta_xO_{12}$ by Al/Ta co-doping. J Solid State Chem. 2021;295.
[6] Thangadurai V, Narayanan S, Pinzaru D. Garnet-type solid-state fast Li ion conductors for Li batteries: critical review. Chem Soc Rev. 2014;43(13):4714–4727.
[7] Rangasamy E, Wolfenstine J, Sakamoto J. The role of Al and Li concentration on the formation of cubic garnet solid electrolyte of nominal composition $Li_7La_3Zr_2O_{12}$. Solid State Ionics. 2012;206:28–32.
[8] Wu JF, Chen E-Y, Yu Y, et al. Gallium-Doped $Li_7La_3Zr_2O_{12}$ garnet-type electrolytes with high lithium-ion conductivity. ACS Appl Mater Interfaces. 2017;9(2):1542–1552.

[9] Ohta S, Kobayashi T, Asaoka T. High lithium ionic conductivity in the garnet-type oxide $Li_{7-X}La_3(Zr_{2-X}, Nb_X)O_{12}$ (X = 0-2). J Power Sources. 2011;196 (6):3342–3345.
[10] Wang YX, Lai W. High ionic conductivity lithium garnet oxides of $Li_{7-x}La_3Zr_{2-x}Ta_xO_{12}$ compositions. Electrochemical and Solid State Letters. 2012;15(5): A68–A71.
[11] Dumon A, Huang M, Shen Y, et al. High Li ion conductivity in strontium doped $Li_7La_3Zr_2O_{12}$ garnet. Solid State Ionics. 2013;243:36–41.
[12] Deviannapoorani C, Shankar LS, Ramakumar S, et al. Investigation on lithium ion conductivity and structural stability of yttrium-substituted $Li_7La_3Zr_2O_{12}$. Ionics. 2016;22(8):1281–1289.
[13] Zhang BK, Tan R, Yang L, et al. Mechanisms and properties of ion-transport in inorganic solid electrolytes. Energy Storage Materials. 2018;10:139–159.
[14] Shao CY, Yu Z, Liu H, et al. Enhanced ionic conductivity of titanium doped $Li_7La_3Zr_2O_{12}$ solid electrolyte. Electrochim Acta. 2017;225:345–349.
[15] Meesala Y, Liao Y-K, Jena A, et al. An efficient multi-doping strategy to enhance Li-ion conductivity in the garnet-type solid electrolyte $Li_7La_3Zr_2O_{12}$. J Mater Chem A. 2019;7(14):8589–8601.
[16] Brugge RH, Kilner JA, Aguadero A. Germanium as a donor dopant in garnet electrolytes. Solid State Ionics. 2019;337:154–160.
[17] Hu ZL, Liu H, Ruan H, et al. High Li-ion conductivity of Al-doped $Li_7La_3Zr_2O_{12}$ synthesized by solid-state reaction. Ceram Int. 2016;42 (10):12156–12160.
[18] Guo SJ, Sun YG, Cao AM. Garnet-type solid-state electrolyte $Li_7La_3Zr_2O_{12}$: crystal structure, element doping and interface strategies for solid-state lithium batteries. Chem Res Chin Univ. 2020;36(3):329–342.
[19] Lan WJ, Fan H, Lau VW-h, et al. Realizing $Li_7La_3Zr_2O_{12}$ garnets with high Li+ conductivity and dense microstructures by Ga/Nb dual substitution for lithium solid-state battery applications. Sustain Energ Fuels. 2020;4(4):1812–1821.
[20] Shen XF, Zhang Q, Ning T, et al. Effects of a dual doping strategy on the structure and ionic conductivity of garnet-type electrolyte. Solid State Ionics. 2020;356.
[21] Ma K, Chen B, Li C-X, et al. Synthesis, structure, transport properties, electrochemical stability window, and lithium plating/stripping of Mg and Nb codoped $Li_7La_3Zr_2O_{12}$ garnet-type solid electrolytes. J Phys Chem C. 2022;126(18):7828–7840.
[22] Wang Y, Wu Y, Wang Z, et al. Doping strategy and mechanism for oxide and sulfide solid electrolytes with high ionic conductivity. J Mater Chem A. 2022;10(9):4517–4532.
[23] Zhang L, Zhuang Q, Zheng R, et al. Recent advances of $Li_7La_3Zr_2O_{12}$-based solid-state lithium batteries towards high energy density. Energy Storage Mater. 2022;49:299–338.
[24] Aktas S, Özkendir OM, Eker YR, et al. Study of the local structure and electrical properties of gallium substituted LLZO electrolyte materials. J Alloys Compd. 2019;792:279–285.
[25] Klysubun W, Tarawarakarn P, Sombunchoo P, et al. X-ray absorption spectroscopy beamline at the Siam Photon Laboratory. Synchrotron Radiat Instrum, Pts 1 and 2. 2007;879:860-+.
[26] Newville M. IFEFFIT: interactive XAFS analysis and FEFF fitting. J Synchrotron Radiat. 2001;8:322–324.
[27] Zhao PC, Wen Y, Cheng J, et al. A novel method for preparation of high dense tetragonal $Li_7La_3Zr_2O_{12}$. J Power Sources. 2017;344:56–61.
[28] Kokal I, Somer M, Notten PHL, et al. Sol-gel synthesis and lithium ion conductivity of $Li_7La_3Zr_2O_{12}$ with garnet-related type structure. Solid State Ionics. 2011;185 (1):42–46.
[29] Allen JL, Wolfenstine J, Rangasamy E, et al. Effect of substitution (Ta, Al, Ga) on the conductivity of $Li_7La_3Zr_2O_{12}$. J Power Sources. 2012;206:315–319.
[30] Sanson A. EXAFS spectroscopy: a powerful tool for the study of local vibrational dynamics. Microstructures. 2021;1(1):2021004.
[31] Ozkendir OM. Crystal and electronic characterization of $Nd_xTi_{1-x}BO_{2+d}$ semiconductors. Mater Res Bull. 2016;74:27–33.
[32] Yin Q, Chen L. Crystallization behavior and electrical characteristics of Ga–Sb thin films for phase change memory. Nanotechnology. 2020;31(21):215709.
[33] Li X, Le Q, Zhou X, et al. The strengthening mechanism and deformation behavior of Mg–Li matrix composite reinforced by Al_3La phase formed in-situ through La_2O_3 particle. Compos Part B: Eng. 2021;216:108866.
[34] Husain H, Sulthonul M, Hariyanto B, et al. Technical aspects of EXAFS data analysis using Artemis software. Mater Today Proc. 2021;44:3296–3300.